# Edinburgh Research Explorer

# Improved radius determinations for the transiting brown dwarf population in the era of Gaia and TESS

# Improved radius determinations for the transiting brown dwarf population in the era of *Gaia* and *TESS*

Theron W. Carmichael ⭐

*Institute for Astronomy, University of Edinburgh, Royal Observatory, Blackford Hill, Edinburgh, EH9 3HJ, UK*

## ABSTRACT

I report updates to the substellar mass–radius diagram for 11 transiting brown dwarfs (BDs) and low-mass stars published before the third data release from the Gaia mission (Gaia DR3). I re-analyse these transiting BD systems whose physical parameters were published between 2008 and 2019 and find that when using the parallax measurements from Gaia DR3, seven BDs show significant differences in their radius estimate or an improvement in the radius uncertainty. This has important implications for how these BDs are used to test substellar evolutionary models in the mass–radius diagram. The remaining four BDs show mass–radius estimates that are consistent with their previous pre-Gaia DR3 measurements. The seven BDs that show significant deviation from the original mass–radius measurements are AD 3116b, CoRoT-3b, CoRoT-15b, EPIC 201702477b, Kepler-39b, KOI-205b, and KOI-415b. Of these, AD 3116b is a known member of the Praesepe cluster at an age of 600 Myr. Additionally, some of the previously smallest known transiting BDs, KOI-205b and KOI-415b, are not as small as once thought, leaving the mass–radius region for the very oldest BDs relatively sparse as a result of this work.

**Key words:** techniques: photometric – techniques: radial velocities – stars: brown dwarfs – stars: low mass.

## 1 INTRODUCTION

The transiting brown dwarf (BD) population has grown at a remarkable rate over the past 4 years due in large part to NASA's Transiting Exoplanet Survey Satellite (*TESS*) mission (Ricker et al. 2015), which was launched in 2018. These discoveries have been especially important because of how well the *TESS* mission has aided in the precise characterization of the fundamental properties, namely the radius, of these transiting BDs. Astronomers have traditionally defined the range of masses for BDs to be between 13 and 80 Jupiter masses ($M_J$), but more thorough studies have determined the mass range to vary between $11–16\,M_J$ at the lower end (Spiegel, Burrows & Milsom 2011) and $75–80\,M_J$ (Baraffe et al. 2003) at the higher end. These thresholds vary by several Jupiter masses because of variations in the chemical composition of the BDs and possibly because of their formation conditions. Some studies even prefer a breakdown by mass density and show a substellar boundary as low as $60\,M_J$ (Hatzes & Rauer 2015). Although a precise mass determination is important to confirm that an object is indeed a BD, a precise radius determination is just as crucial. One of the best ways we can precisely determine the radius of a BD is by searching for transiting BD systems. Of the 37 known transiting BD systems, we typically find them to have radii between 0.7 and 1.4 Jupiter radii ($R_J$) (Carmichael et al. 2021; Grieves et al. 2021).

While we use spectra and radial velocities (RVs) of host stars to precisely measure the mass of a transiting BD, we use transits of main sequence stars by BDs that provide an estimate of the radius of a BD. The precision of this estimate is directly impacted by how well we know the host star's radius as the transit depth is $\delta \propto (R_b/R_\star)^2$. Until recently, this knowledge of the host star's radius has been a frequent limiting factor on the ultimate precision and accuracy to which we could know the radii of transiting BDs.

This is where the Gaia mission has played a pivotal role in our estimation of transiting BD radii. With the Gaia mission's third data release, we now have access to precise and accurate parallaxes for all of the main sequence stars that are known to host transiting BDs. These parallaxes directly translate into stellar distances and radii (via the distance–luminosity relation $L_\star \propto d^2$), which means that these stellar radii are no longer as much of a limiting factor as before Gaia DR3. However, this means that a number of transiting BDs published previous to the launch of the Gaia mission will not have as precise or accurate stellar (and BD) radii as is currently possible. In fact, nearly a dozen different transiting BD systems published prior to 2019 have inaccurate or no parallax information for the host star of the BD. This practice of re-analysing transiting BDs has been established in the past with systems like WASP-30, where Triaud et al. (2013) provided improved mass–radius measurements over the original discovery work by Anderson et al. (2011). A similar improvement in work was done by Bonomo et al. (2015) for the Kepler-39 and KOI-205 transiting BD systems. Other works that re-analyse previously known systems from the wider exoplanet community are Schanche et al. (2020) and Borsato et al. (2021).

It is particularly important that these radius measurements are updated as they most directly enable us to make some conclusion of a transiting BD's age. This is because BDs – transiting or not – are believed to contract with age (Burrows et al. 2001; Baraffe et al.

⭐ E-mail: tcarmich@ed.ac.uk

2003; Phillips et al. 2020; Marley et al. 2021) and the rate of this contraction is of key interest to those who simulate the evolution of BDs. The radius of transiting BDs aids us in distinguishing young BDs from old BDs just like the mass of a BD distinguishes them from giant planets and low-mass stars.

Age is a particularly difficult parameter to measure for stars, let alone transiting BDs, but previous works have been able to determine relatively precise ages for transiting BD systems. For example, Carmichael et al. (2021) used gyrochronology of a young solar analogue host star to constrain the age of a transiting BD. Others like Gillen et al. (2017), Nowak et al. (2017), and David et al. (2019) have determined the ages of transiting BDs via associating their host stars with stellar clusters, for which we typically know the ages very well. It is these systems where the star's age is so precisely known that are the most important to have a precise and accurate radius for the transiting BD. This enables a well-informed examination of how well BD evolutionary models are able to predict the radius evolution of BDs and so allow for deeper investigations into other BD properties like chemical composition and internal structure.

Here I show updated estimates of the masses and radii of 11 different transiting BD systems that were published between 2008 and 2019. These 11 systems are AD 3116, CoRoT-3, CoRoT-15, EPIC 201702477, KELT-1, Kepler-39, KOI-189, KOI-205, KOI-415, WASP-30, and WASP-128. Of these, I provide improved mass and radius estimates for AD 3116b, CoRoT-3b, CoRoT-15b, EPIC 201702477b, Kepler-39b, KOI-205b, and KOI-415b. Section 2 will present the new *TESS* observations used for a number of these systems and review the previously published data, and, in one case, point out erroneous information. Section 3 will present the tools used to re-analyse these systems and show agreement with or improvements to previously published mass–radius determinations. Section 4 will provide discussion on specific systems to compare them to their previously published values and will also remark on how the improved mass–radius determinations affect the substellar mass–radius diagram.

## 2 OBSERVATIONS

Here I present the new *TESS* light curve analysis I performed for a subset of these transiting BD systems. I also briefly review the provenance of the originally published light curve and RV data for each system. I use these data in most cases for the re-analysis of the systems in this work.

### 2.1 *TESS* data

I use light curve data from *TESS* for 5 of the 11 transiting BDs that are part of this work. In some cases, the *TESS* light curves are in addition to the original discovery light curves. Unless explicitly stated otherwise, I use the Science Processing Operations Center (SPOC; Jenkins et al. 2016) *TESS* light curves that are available on the *Mikulski Archive for Space Telescopes* (MAST). These data are from the Presearch Data Conditioning Simple Aperture Photometry flux pipeline (PDCSAP; Smith et al. 2012; Stumpe et al. 2014), which removes some systematic stellar effects but aims to retain transits, eclipses, and native stellar features such as brightness modulation. I then use the `lightkurve` (Lightkurve Collaboration 2018) package in Python to normalize the PDCSAP light curves for transit analysis, which typically involves removing photometric modulation caused by star spots and stellar rotation. All 11 systems have been observed by *TESS* for at least one sector, but not every

**Table 1.** Object names, observed *TESS* sectors, and observation cadence (in seconds) as of August 2022 (Sector 54). The bold numbers in the 'Sectors Obs' column indicate which *TESS* sectors the data used in this work originate from. Though EPIC 201 702 477 was observed by *TESS* and processed through the SPOC pipeline, the transits of the BD were not captured due to the breaks in the light curve data. The transits of CoRoT-15b are completely diluted by neighbouring stars, with one at 23.8 arcsec with a $\Delta G = -0.4$ (fainter) magnitudes and 2 at 30–40 arcsec with a $\Delta G = +1$-2 (brighter) magnitudes. Objects with the 'No SPOC' note were not processed through the SPOC PDCSAP pipeline or not currently made available at MAST. This means that the spacecraft motions and scattered Earth and moon light from the affected *TESS* sectors are not removed from the raw light curves, so I do not use them.

| Object name | TIC ID | Sectors obs | Cadence (s) |
|---|---|---|---|
| AD 3116 | 184 892 124 | **44**, **45**, **46** | 120 |
| CoRoT-3 | 392 353 449 | **54** | 120 |
| CoRoT-15 | 206 893 389 | 6, 33 | No detection |
| EPIC 201 702 477 | 281 888 055 | 45, 46 | No detection |
| KELT-1 | 432 549 364 | **17** | 120 |
| Kepler-39 | 272 836 943 | 14, 15, 41 | No SPOC |
| KOI-189 | 48 451 130 | 14, 15, 26, **40**, **41** | 120 |
| KOI-205 | 271 749 758 | 14, 15, 40, 41 | No SPOC |
| KOI-415 | 138 099 073 | 14, 15, 40, 41 | No SPOC |
| WASP-30 | 9 725 627 | **2**, **29**, **42** | 120, 600 |
| WASP-128 | 180 991 313 | **10**, **36**, **37** | 600 |

light curve produced is suitable for transit analysis. I restrict the use of *TESS* data for transit analysis to those systems with *TESS* data that have been processed through the PDCSAP pipeline. This means that only AD 3116, CoRoT-3, KELT-1, KOI-189, WASP-30, and WASP-128 use *TESS* data in this work. The remaining systems (CoRoT-15, Kepler-39, KOI-205, and KOI-415) suffer from dilution from nearby stars or do not have light curve data processed by SPOC at the time of this work. For these systems, the algorithms in Smith et al. (2012) and Stumpe et al. (2014) would need to be replicated here in order to correct for spacecraft motions and scattered Earth and moon light contamination prevalent in certain *TESS* sectors (most notably the *Kepler* field for this work). I avoid this level of raw data reduction as it would not be of the same quality as that from SPOC and it could introduce inconsistent or inadequate treatment of these systems. The light curves from SPOC vary in cadence as they are sometimes sourced from the *TESS* full-frame images, which change in their exposure times between the primary and extended *TESS* missions.

The new *TESS* data used in this work are detailed in Table 1 with the sectors each target was observed in along with the cadence (exposure times) for the light curve data.

### 2.2 CoRoT brown dwarfs

I use the light curve data from the CoRoT mission (Baglin et al. 2006) along with the respective RV data published for the analysis of CoRoT-3 (Deleuil et al. 2008) and CoRoT-15 (Bouchy et al. 2011a). CoRoT-3 has RV data from the CORALIE, HARPS, Sandiford, SOPHIE, and TLS instruments while CoRoT-15 has RV data from HARPS and HIRES only. The *TESS* data for CoRoT-15 are too diluted from nearby starlight to be of use here. This is partly due to the design of the CoRoT mission as its pixel scale of 2.32 arcsec is much better than *TESS* at observing the relatively crowded fields of stars that CoRoT-15 occupies. Though the *TESS* light curve of CoRoT-3 is also diluted, the transits are still recoverable, so I use these data in my analysis.

**Table 2.** Corrected BJD values for KOI-189 RVs from the SOPHIE spectrograph.

| BJD (days) | RV (m s$^{-1}$) | RV uncertainty (m s$^{-1}$) |
|---|---|---|
| 2455746.4495 | −78748.0 | 24.0 |
| 2455763.5061 | −68845.0 | 16.0 |
| 2455768.4028 | −71854.0 | 13.0 |
| 2455773.4533 | −75930.0 | 34.0 |
| 2455776.5059 | −78475.0 | 36.0 |
| 2455785.4191 | −69234.0 | 30.0 |
| 2455788.5163 | −67503.0 | 59.0 |
| 2455791.4151 | −67779.0 | 37.0 |
| 2455809.3730 | −79241.0 | 51.0 |
| 2455876.2423 | −69533.0 | 56.0 |

### 2.3 *Kepler* and *K2* brown dwarfs

#### 2.3.1 Kepler

Of the four transiting BD systems discovered by the *Kepler* mission (Borucki et al. 2010), only KOI-189 has a *TESS* light curve that is vetted by the SPOC. I include these data in addition to the original light curve data from Díaz et al. (2014) for KOI-189 in the transit analysis while I use the original *Kepler* data from Bonomo et al. (2015), Díaz et al. (2013), and Moutou et al. (2013) for Kepler-39, KOI-205, and KOI-415, respectively. I use the RV data from SOPHIE instrument originally published for Kepler-39, KOI-205, and KOI-415.

The RV data from the SOPHIE instrument for KOI-189 have erroneous observations times as presented in Díaz et al. (2014). I show the corrected values in Table 2. The error in the observation times (BJD) was a typographical mistake in the hundred-thousands place where the '4' was incorrectly replaced with a '5' (as in 2,405,746 to 2,505,746). Taken as shown in Díaz et al. (2014), these RV data would be dated on May 2148, and not June 2011 as the original paper states within the text accompanying the table.

#### 2.3.2 K2

The transiting BD systems from the *K2* mission (Howell et al. 2014) are AD 3116 (EPIC 211946007) and EPIC 201702477. There are data from *TESS* for both of these systems, but only AD 3116 shows evidence of a transit; the *TESS* mission does not detect transits for the EPIC 201 702 477 system across the two consecutive sectors it was observed in. This is likely because of the 41-day orbital period of this BD and the breaks in the *TESS* data. Given this, only the *TESS* data for AD 3116, in addition to the light curve data from Gillen et al. (2017), are used for the transit analysis while just the light curve data from *K2* and ground-based facilities (Bayliss et al. 2017) are used for EPIC 201702477. These ground-based facilities are the Cerro Tololo InterAmerican Observatory (CTIO) and the South African Astronomical Observatory (SAAO). I use the RV data from these previous works for this pair of *K2* systems (*Keck*/HIRES for AD 3116; HARPS and SOPHIE for EPIC 201702477).

### 2.4 KELT and WASP brown dwarfs

#### 2.4.1 KELT

The single transiting BD system from the KELT survey (Pepper et al. 2007) is KELT-1 (Siverd et al. 2012). I use the *TESS* data in addition to the ground-based data originally published for the transit analysis of this system. The ground-based light curve data are from

the University of Louisville Moore Observatory (ULMO/MORC24) and the Fred Lawrence Whipple Observatory (FLWO/KeplerCam) and the RV data are from the TRES instrument at FLWO.

#### 2.4.2 WASP

The WASP survey (Pollacco et al. 2006) has detected two transiting BD systems, WASP-30 and WASP-128. I use the light curve from the TRAPPIST telescope and RV data from CORALIE for the analysis of WASP-30 (Triaud et al. 2013). I note that *TESS* data from SPOC are available for both WASP-30 and WASP-128, but, given the photometric modulation of WASP-30's light curve, the resulting normalized *TESS* light curve shows a slightly shallower transit compared to the TRAPPIST light curve, so this required additional use of spline detrending tools in `lightkurve`. In the case of WASP-128, I use the original RV data from CORALIE and HARPS (Hodžić et al. 2018), but not the original light curve data, as these were not made available. Instead, I use the *TESS* data for the transit analysis of WASP-128.

## 3 ANALYSIS

### 3.1 Global analysis with `EXOFASTv2`

Here I give details on my global analysis of the stellar and BD parameters for these 11 systems using `EXOFASTv2` (Eastman et al. 2019). `EXOFASTv2` uses the Monte Carlo–Markov Chain (MCMC) method to estimate the most likely values and uncertainties for the physical properties of the star and BD in each system. I use $N = 36$ ($N = 2 \times n_{parameters}$) walkers, or chains, and run until the fit passes the default convergence criteria for `EXOFASTv2`, which is typically on the order of hundreds of thousands of steps for these systems (described in more detail in Eastman et al. 2019).

I set either uniform $\mathcal{U}[a, b]$ or Gaussian $\mathcal{G}[a, b]$ priors on the following input parameters: parallax ($\varpi$) from Gaia DR3, spectroscopic stellar effective temperature ($T_{eff}$), spectroscopic stellar metallicity ([Fe/H]), and V-band extinction ($A_V$). The two spectroscopic priors are taken from the respective results in the discovery works for each system and an upper limit is set on $A_V$ from a database[1] with measurements from Schlafly & Finkbeiner (2011). Of these priors, $\varpi$ in particular aids in establishing a precise estimate for the stellar radius, which directly affects the estimate for the BD radius. Following the method detailed in Lindegren et al. (2021), I apply the parallax zero-point correction to the Gaia DR3 $\varpi$. The systems in this paper experience a 1–2$\sigma$ change in $\varpi$ when the correction is applied,[2] except for AD 3116, which only sees a $\Delta\varpi \approx 0.25\sigma$.

In addition to these priors, I input the following data with `EXOFASTv2`: magnitude measurements of the host star for the SED (shown in Tables 3 and 4), previously published RV data for each system, and new *TESS* light curves and previously published light curves. In some cases, the light curve data are truncated to only include the transit events with 4–5 hours of baseline before ingress and after egress. This is done to reduce the convergence time for systems with especially long temporal coverage by space telescope missions. This should not be done if a search for secondary eclipses has not been performed as secondary eclipse data provide valuable

---

[1] Database for extinction calculation: https://irsa.ipac.caltech.edu/frontpage/
[2] Gaia parallax zero-point correction code: https://www.cosmos.esa.int/web/gaia/edr3-code

**Table 3.** Table of magnitudes used in SED fitting for the host stars in AD 3116, CoRoT-3, CoRoT-15, EPIC 201702477, and KELT-1. Sources: *Gaia* – Gaia Collaboration (2022), *TESS* – Stassun et al. (2018), 2MASS – Skrutskie et al. (2006), WISE – Wright et al. (2010). Additional magnitudes for AD 3116 and EPIC 201 702 477 are sourced from Gillen et al. (2017) and Bayliss et al. (2017), respectively.

|  | AD 3116 | CoRoT-3 | CoRoT-15 | EPIC 201 702 477 | KELT-1 |
|---|---|---|---|---|---|
| *TESS* | 16.057 ± 0.008 | 12.713 ± 0.011 | 14.869 ± 0.008 | 13.920 ± 0.007 | 10.224 ± 0.006 |
| $G$ | 17.416 ± 0.020 | 13.219 ± 0.020 | 15.599 ± 0.001 | 14.391 ± 0.001 | 10.591 ± 0.001 |
| $G_{BP}$ | 19.084 ± 0.026 | 13.623 ± 0.020 | 16.240 ± 0.020 | 14.764 ± 0.020 | 10.873 ± 0.020 |
| $G_{RP}$ | 16.147 ± 0.020 | 12.652 ± 0.020 | 14.823 ± 0.020 | 13.863 ± 0.020 | 10.175 ± 0.020 |
| $J$ | - | 11.936 ± 0.030 | 13.801 ± 0.030 | 13.268 ± 0.030 | 9.682 ± 0.020 |
| $H$ | - | 11.710 ± 0.040 | 13.434 ± 0.040 | 12.881 ± 0.030 | 9.534 ± 0.030 |
| $K_S$ | 13.499 ± 0.043 | 11.618 ± 0.030 | 13.389 ± 0.050 | 12.766 ± 0.030 | 9.437 ± 0.020 |
| WISE1 | 13.330 ± 0.030 | 11.343 ± 0.030 | 13.168 ± 0.030 | 12.814 ± 0.030 | 9.414 ± 0.030 |
| WISE2 | 13.113 ± 0.030 | 11.394 ± 0.030 | 13.141 ± 0.032 | 12.840 ± 0.030 | 9.419 ± 0.030 |
| WISE3 | – | 11.323 ± 0.172 | 12.152 ± 0.435 | – | 9.386 ± 0.034 |
| $u$ | 22.290 ± 0.190 | – | – | 16.312 ± 0.005 | – |
| $g$ | 19.646 ± 0.014 | – | – | 14.871 ± 0.003 | – |
| $r$ | 16.675 ± 0.005 | – | – | 14.354 ± 0.003 | – |
| $z$ | 15.845 ± 0.006 | – | – | 14.137 ± 0.004 | – |

**Table 4.** Table of magnitudes used in SED fitting for the host stars in Kepler-39, KOI-189, KOI-205, KOI-415, WASP-30, and WASP-128. Sources: *Gaia* – Gaia Collaboration (2022), *TESS* – Stassun et al. (2018), 2MASS – Skrutskie et al. (2006), WISE – Wright et al. (2010).

|  | Kepler-39 | KOI-189 | KOI-205 | KOI-415 | WASP-30 | WASP-128 |
|---|---|---|---|---|---|---|
| *TESS* | 13.826 ± 0.001 | 13.759 ± 0.001 | 13.935 ± 0.008 | 13.662 ± 0.007 | 10.977 ± 0.008 | 11.867 ± 0.006 |
| $G$ | 14.262 ± 0.020 | 14.380 ± 0.020 | 14.511 ± 0.020 | 14.114 ± 0.020 | 11.350 ± 0.020 | 12.274 ± 0.020 |
| $G_{BP}$ | 14.598 ± 0.020 | 14.926 ± 0.020 | 14.999 ± 0.020 | 14.467 ± 0.020 | 11.640 ± 0.020 | 12.583 ± 0.020 |
| $G_{RP}$ | 13.764 ± 0.020 | 13.703 ± 0.020 | 13.882 ± 0.020 | 13.604 ± 0.020 | 10.934 ± 0.020 | 11.814 ± 0.020 |
| $J$ | 13.236 ± 0.030 | 12.895 ± 0.030 | 13.095 ± 0.020 | 13.049 ± 0.020 | 10.508 ± 0.030 | 11.282 ± 0.020 |
| $H$ | 12.999 ± 0.020 | 12.377 ± 0.020 | 12.709 ± 0.020 | 12.671 ± 0.020 | 10.283 ± 0.020 | 11.011 ± 0.020 |
| $K_S$ | 12.918 ± 0.030 | 12.288 ± 0.030 | 12.656 ± 0.020 | 12.661 ± 0.030 | 10.199 ± 0.020 | 10.942 ± 0.020 |
| WISE1 | 12.858 ± 0.030 | 12.239 ± 0.030 | 12.579 ± 0.030 | 12.571 ± 0.030 | 10.162 ± 0.030 | 10.923 ± 0.030 |
| WISE2 | 12.892 ± 0.030 | 12.327 ± 0.030 | 12.685 ± 0.030 | 12.595 ± 0.030 | 10.202 ± 0.030 | 10.936 ± 0.030 |
| WISE3 | 12.601 ± 0.329 | 12.280 ± 0.233 | 12.396 ± 0.294 | 12.364 ± 0.289 | 10.077 ± 0.060 | 10.966 ± 0.088 |

information on the nature of the companion. I let the RV offset $\gamma$ be a free parameter and use the RV jitter term, $\sigma_J$, to account for the surface activity of the star. The RV jitter term is based on a simple white noise model implemented in EXOFASTv2. The stellar magnitudes along with the input spectroscopic data establish the boundaries on the MIST stellar isochrone models (Paxton et al. 2015; Choi et al. 2016; Dotter 2016) built into EXOFASTv2 and are used here to estimate the stellar parameters for each system.

Full tables describing priors and results are given in the Appendix section. Fig. 1 shows the SED models, Fig. 2 shows the transit models, and Fig. 3 shows the RV orbital solutions.

### 3.2 Treating the AD 3116 system

Unlike every other system in this study, the AD 3116 system contains an M-dwarf primary star that is situated within a star cluster, Praesepe. This means that I may use prior information on the age of the system, $\tau = 617 \pm 17$ Myr from Gossage et al. (2018), and that I must invoke M-dwarf mass–magnitude relations from Mann et al. (2019). I use equation (4) from Mann et al. (2019) to set a mass prior based on the absolute $M_{K_S}$ magnitude, which I convert to from the apparent magnitude shown in Table 3. This

stellar mass prior is set in addition to the general priors mentioned in Section 3.1.

## 4 DISCUSSION

This work has seen an improvement in the mass–radius determinations for seven transiting BDs: AD 3116b, CoRoT-3b, CoRoT-15b, EPIC 201702477b, Kepler-39b, KOI-205b, and KOI-415b. These systems show a reduction in their BD radius uncertainty, a $1\sigma$ or more change in their BD radius, or both of these, which changes the overall composition of the substellar mass–radius diagram (Fig. 4). For the systems whose mass–radius measurements I find to be consistent with previous works (KELT-1, KOI-189, WASP-30, WASP-128), a notable improvement to those are the updated transit timings with *TESS* data. These updated ephemerides will reduce the mid-transit time uncertainty for future works.

I focus on quantifying these improvements in terms of the BD radius as this is a characteristic by which BDs change significantly over their lifetimes and is also measurable via transit photometry. Now that astronomers are able to measure the radii of BDs to a precision of 3–5 per cent, it is important that substellar evolutionary models have a similar or better precision for the radii they predict. If these models can accurately and precisely predict the radius of a
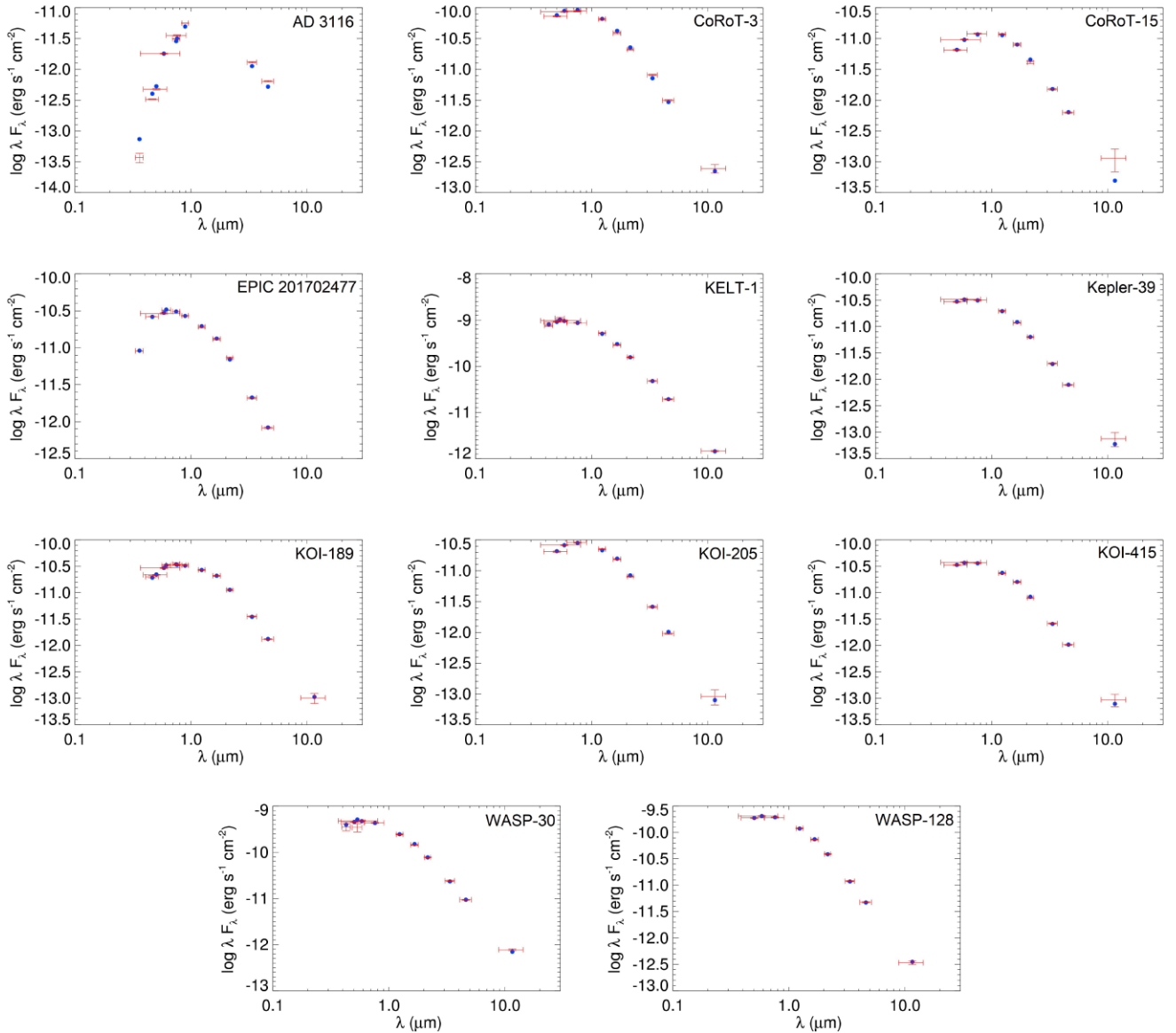
**Figure 1.** SEDs computed using the MIST models built into EXOFASTv2. The blue dots represent the model values and the red crosses are the data from Tables 3 and 4. The most challenging SED to model is that of AD 3116, given that the host star's mass places it near the lower boundaries of what the MIST framework was designed for.

BD in scenarios where the age is known, then other radius-altering factors like metallicity and inflation via stellar irradiation can be more easily explored. This is especially relevant in cases where low-mass transiting BDs may experience inflation caused by irradiation (e.g. Siverd et al. 2012; Benni et al. 2020). Table 5 provides a breakdown of the changes in BD radius values from previous works to this work. This focus on radius is not meant to imply that the mass of these BDs is unimportant, but in general, the mass of the BD is fairly static over the lifetime of the object and age–mass relations show little change compared to age–radius relations for these objects.

I also highlight the specific systems that show significant changes in agreement with age–radius predictions from substellar evolutionary models from Phillips et al. (2020), referred to as the ATMO 2020 models, and the Baraffe et al. (2003) models, referred to as the COND03 models. These systems are Kepler-39, KOI-205, KOI-415, and EPIC 201702477. The changes in agreement are

sometimes in favour of the models and sometimes not, depending on the system. Though other frameworks for substellar evolutionary models exist and take a different approach to BD radius evolution (e.g. Marley et al. 2021), I limit my comparisons to the ATMO 2020 and COND03 models for the sake of simplicity and to focus broadly on how these types of models match up against the transiting BD population, especially the oldest and smallest known transiting BDs.

### 4.1 Specific changes to each brown dwarf system

Here I will provide details for each system and, where appropriate, highlight the sources of significant changes in the radius or radius precision of these transiting BD systems. In several cases, my results are consistent with previous works, so those original works should be used when referencing the stellar and BD parameters for those systems.
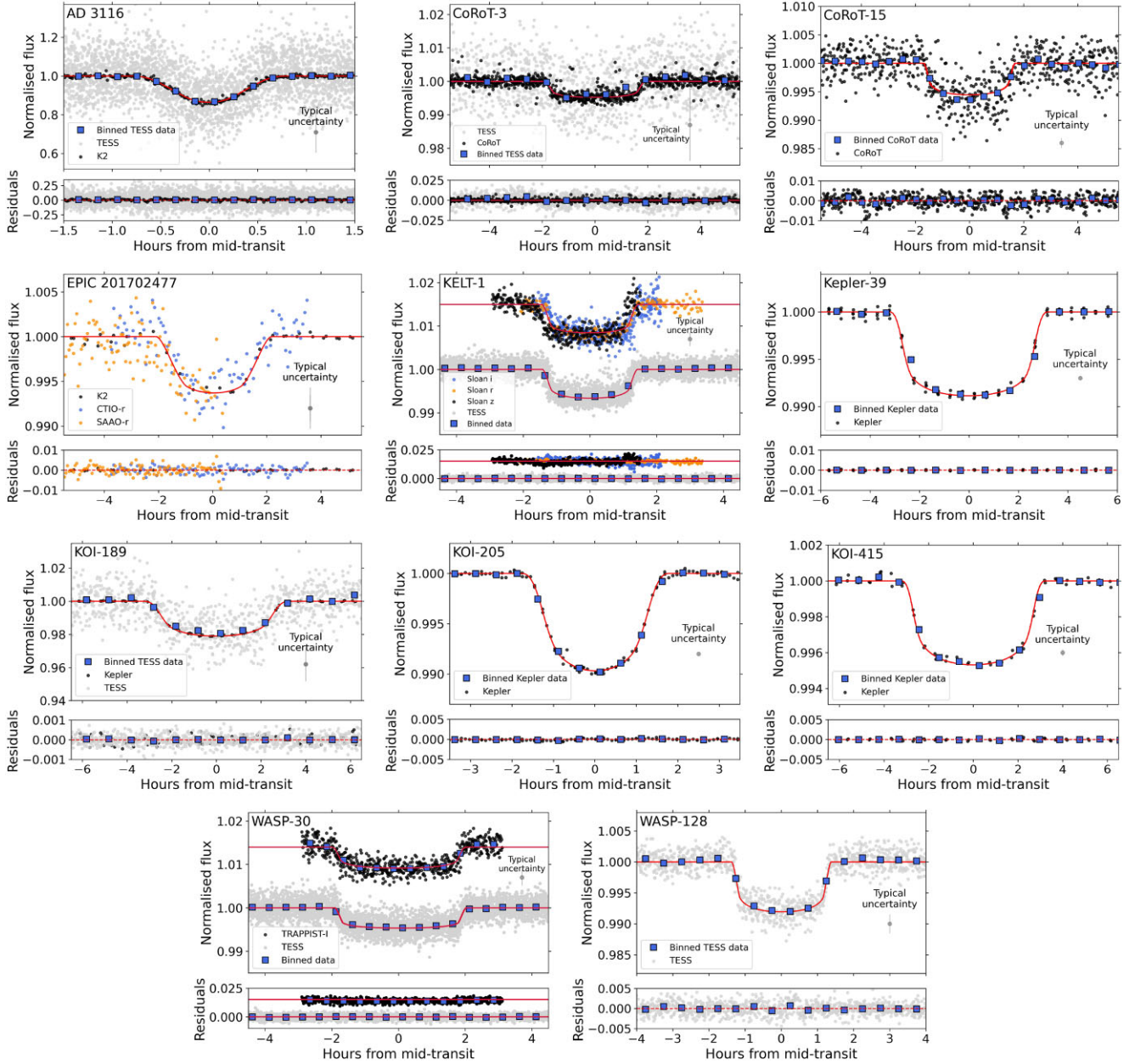
**Figure 2.** Transit light curves modelled in this study. The red curve indicates the best-fitting model for each transit.

### 4.1.1 AD 3116

The original discovery paper for AD 3116 by Gillen et al. (2017) uses the parallax measurement to the star cluster, Praesepe, from Gaia DR1, which translates to a distance of $d = 182.8 \pm 1.7 \pm 14$ pc, where the second uncertainty measurement represents the observed radial spread of high-probability members of the cluster on the sky. In Gillen et al. (2017), they choose $d = 182.8 \pm 14$ pc for this system and so are limited to a worse precision on the radius of the host star and radius of the BD. Using the relations from Mann et al. (2019) along with the Gaia DR3 parallax measurement ($\varpi = 5.39 \pm 0.14$ mas, $d = 185.4 \pm 4.8$ pc), I find an uncertainty on the stellar radius that is a factor of roughly 3 times smaller than that in Gillen et al. (2017), which translates to a 3–4 times reduction in the BD radius uncertainty. I find a more precise radius measurement for AD 3116b to be $R_b = 0.95 \pm 0.07 R_J$, which also improves its consistency with age–radius

relations for BDs between 500 and 600 Myr from ATMO 2020 and COND03. The mass of the BD that I find, $M_b = 54.6 \pm 6.8 M_J$, is slightly less precise, but still consistent with the BD mass found in Gillen et al. (2017) ($M_b = 54.2 \pm 4.3 M_J$).

### 4.1.2 CoRoT-3

CoRoT-3 is the first-known transiting BD and in Deleuil et al. (2008), they report a stellar distance and radius of $680 \pm 160$ pc and $R_\star = 1.56 \pm 0.09 R_\odot$, respectively. The distance derived from Gaia DR3 in this work is $764 \pm 10$ pc, which effectively translates to a larger host star ($R_\star = 1.66 \pm 0.08 R_\odot$) at a further distance compared to the original findings. The larger measurement for the host yields a larger radius measurement for the BD of $R_b = 1.08 \pm 0.05 R_J$. I find that the mass $M_b = 22.3 \pm 1.0 M_J$ of CoRoT-3b is consistent with
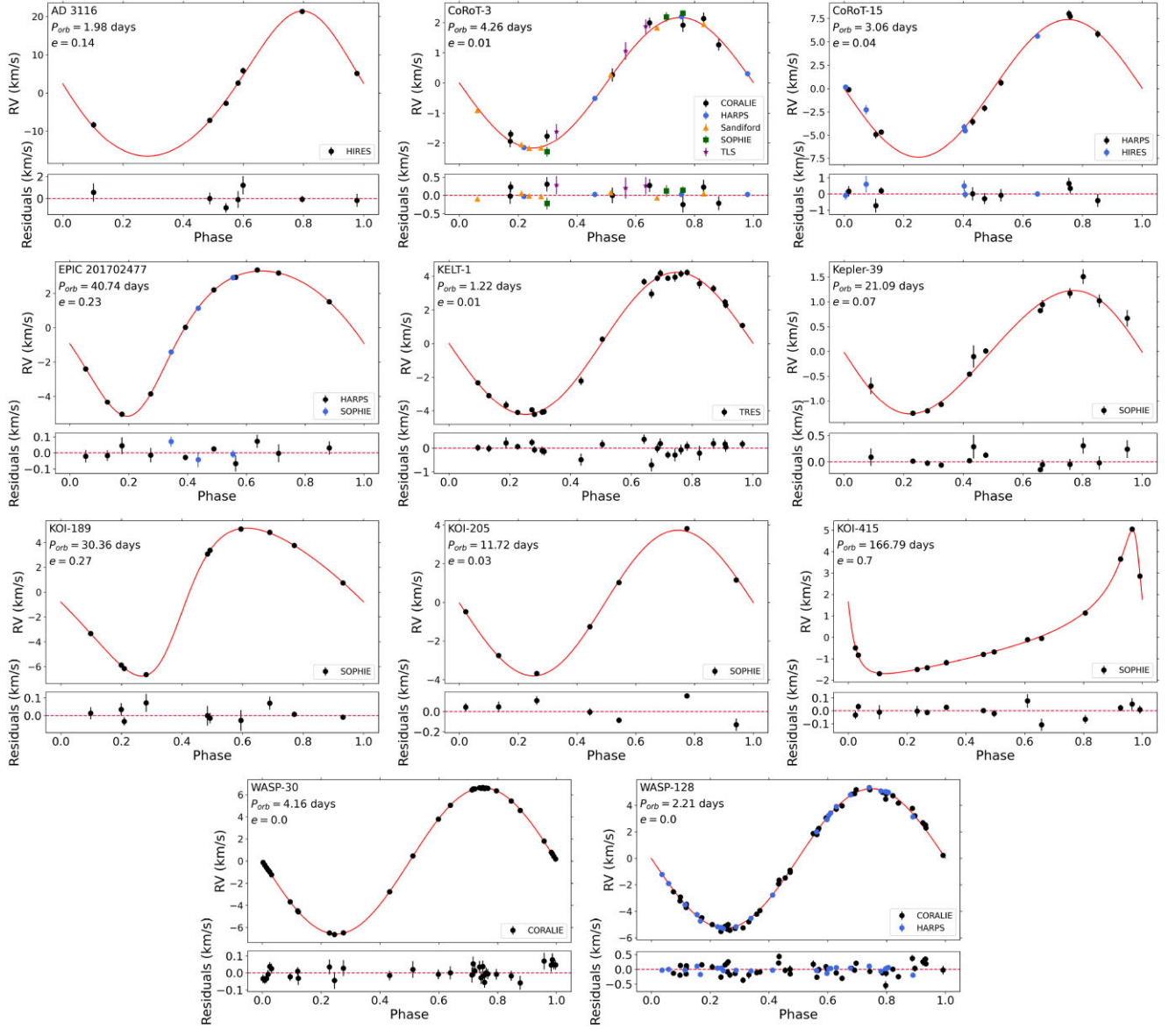
**Figure 3.** Relative RV measurements for the systems analysed in this work. The red curve indicates the best-fitting orbital solution. These data are sourced from their respective discovery works with the exception of KOI-189, which has had the BJD values altered due to a typographical error in the original work. Table 2 gives the corrected BJD values.

the value in the original work. Given its mass–radius position in Fig. 4, CoRoT-3b seems to be among the group of inflated transiting BDs, like GPX-1b (Benni et al. 2020) and KELT-1b (Siverd et al. 2012), where those systems have strong evidence for radius inflation due to their proximity to their host star.

### 4.1.3 CoRoT-15

The second ever-known transiting BD, CoRoT-15b initially held one of the largest radius uncertainty estimates for transiting BDs at 27 per cent ($R_b = 1.12 \pm 0.30 R_J$). With such a large radius uncertainty, this BD was not a particularly useful test of substellar isochrones in the mass–radius diagram. Bouchy et al. (2011a) estimate the distance to CoRoT-15 to be $d = 1270 \pm 300$ pc, which is slightly closer than the distance derived from Gaia DR3 of $d = 1367 \pm 130$ pc. However, the primary source of the large

radius uncertainty on the BD in Bouchy et al. (2011a) is the stellar radius uncertainty, which is reduced by a factor of 2 in this work. I attribute this to improved stellar evolutionary models from MIST since the original publication of CoRoT-15 in 2011. I find the revised radius for CoRoT-15b is $R_b = 0.94 \pm 0.12 R_J$. Though improved, the radius uncertainty is still somewhat large, which makes the use of this transiting BD as a test for substellar mass–radius models challenging at best.

### 4.1.4 EPIC 201702477

The discovery work for this system by Bayliss et al. (2017) does not explicitly state a parallax or distance to the host star, so the provenance in the differences between my stellar radius measurement ($R_\star = 1.01 R_\odot$) and the measurement from Bayliss et al. (2017) ($R_\star = 0.90 R_\odot$) is not directly traceable to an inaccuracy in one

**Table 5.** Comparison of transiting BD radius values ($R_b$) of this work to pre-Gaia DR2 work (except for WASP-128b, which was published previously using Gaia DR2 data). The $\Delta\sigma_{R_J}$ column quantifies the difference between the previous radius measurements and the measurements using data from Gaia DR3 in this work. Values that are most consistent with each other have $\Delta\sigma_{R_J} < 1.0\sigma$. A visual representation of these results are given in the Appendix.

| Object name | Previous work ($R_J$) | This work ($R_J$) | $\Delta\sigma_{R_J}$ |
|---|---|---|---|
| AD 3116b | $1.02 \pm 0.28$ | $0.95 \pm 0.07$ | $0.98\sigma$ |
| CoRoT-3b | $1.01 \pm 0.07$ | $1.08 \pm 0.05$ | $1.44\sigma$ |
| CoRoT-15b | $1.12 \pm 0.30$ | $0.94 \pm 0.12$ | $1.83\sigma$ |
| EPIC 201702477b | $0.76 \pm 0.07$ | $0.83 \pm 0.04$ | $1.84\sigma$ |
| KELT-1b | $1.11 \pm 0.03$ | $1.13 \pm 0.03$ | $0.66\sigma$ |
| Kepler-39b | $1.22 \pm 0.12$ | $1.07 \pm 0.03$ | $5.67\sigma$ |
| KOI-189b | $1.00 \pm 0.02$ | $0.99 \pm 0.02$ | $0.49\sigma$ |
| KOI-205b | $0.81 \pm 0.02$ | $0.87 \pm 0.02$ | $2.61\sigma$ |
| KOI-415b | $0.79 \pm 0.12$ | $0.86 \pm 0.03$ | $2.80\sigma$ |
| WASP-30b | $0.95 \pm 0.03$ | $0.96 \pm 0.03$ | $0.43\sigma$ |
| WASP-128b | $0.94 \pm 0.02$ | $0.96 \pm 0.02$ | $1.21\sigma$ |

201 702 477 at $6.4 \pm 4.6$ Gyr does not have any better precision than that of Bayliss et al. (2017).

### 4.1.5 KELT-1

The mass–radius determination made by Siverd et al. (2012) stands up to a re-analysis of the KELT-1 system using Gaia DR3. That is to say, I find the original mass–radius value of KELT-1b to be consistent with the values I present here. The original estimate of the distance to KELT-1 nearly exactly matches that from Gaia DR3, so the stellar luminosity and radius measurements were accurate in the original work. As Siverd et al. (2012) conclude, KELT-1b is a transiting BD whose radius has been inflated as a result of the proximity to its host star. I also note that the KELT-1 system has been extensively studied (e.g. Beatty et al. 2017, 2019; Parviainen et al. 2022) in large part due to the accessibility of the host star (it is bright at $V = 10.6$) and the strongly detected secondary eclipses of the BD. In the most recent study of KELT-1, Parviainen et al. (2022) find that the secondary eclipse depth varies greatly between the *TESS* and CHEOPS (Benz et al. 2021) mission data, despite these data being taken in largely overlapping bandpasses. A discussion and analysis of the secondary eclipse of KELT-1b would be redundant here and is beyond the scope of this work. Nonetheless, this aspect of the KELT-1 system is worthy of acknowledgement.

In my work here, Siverd et al. (2012), and Parviainen et al. (2022), we each find a radius for KELT-1b to be $R_b = 1.116 \pm 0.038\,R_J$, $R_b = 1.129 \pm 0.031\,R_J$, and $R_b = 1.138 \pm 0.010\,R_J$, respectively.

### 4.1.6 Kepler-39

The largest discrepancy in BD radius between this work and previous works is seen in the Kepler-39 system. The BD in the Kepler-39 system sees a 10 per cent decrease in radius from $R_b = 1.22 \pm 0.12\,R_J$ to $R_b = 1.07 \pm 0.03\,R_J$. This is a result of the stellar radius decreasing by a similar amount as a result of the application of Gaia DR3 parallax measurements to the system and not any particular improvement to the analysis of the transit events of the BD. The discovery paper (Bouchy et al. 2011b) and the follow-up study (Bonomo et al. 2015) both discuss an over-inflated radius of the transiting BD when compared to the COND03 models by Baraffe et al. (2003), but this no longer seems to be a point of concern with the updated radius that
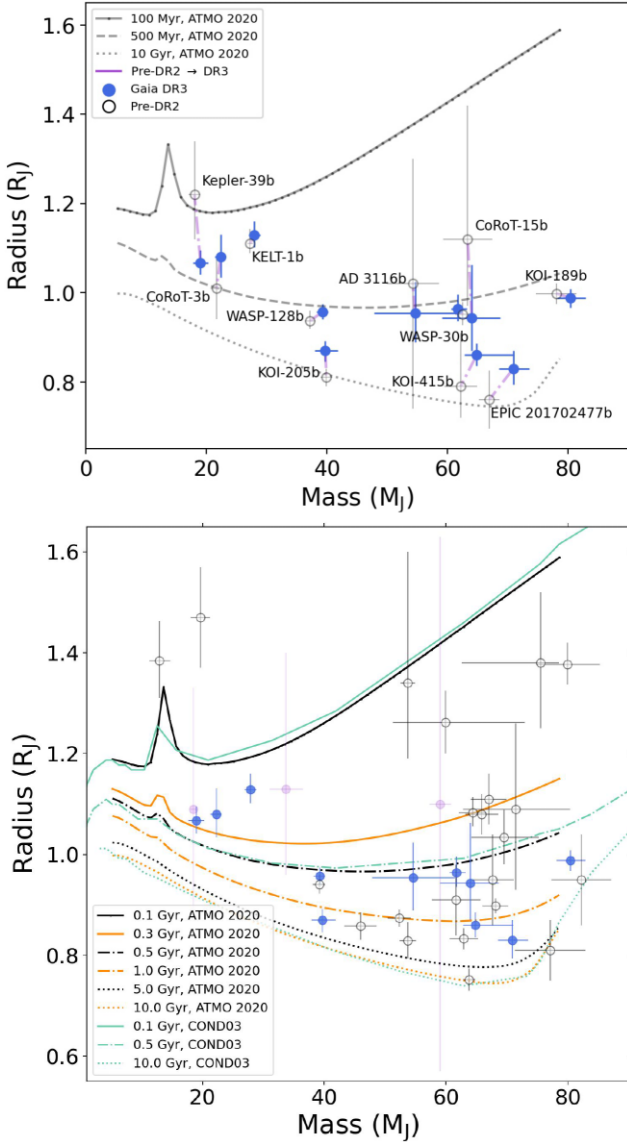
**Figure 4.** *Top*: Mass–radius diagram showing comparison between previous works and this work. The purple line connects the measurements made by previous works (open circles) to this work (blue filled circles). Another visual breakdown of this comparison is shown in Figs A1 and A2. *Bottom*: The complete known transiting BD population as of August 2022. This excludes eclipsing binary BDs and BDs that transit white dwarf hosts. The blue points show the systems re-analysed with Gaia DR3 information in this work and the faded purple points indicate transiting BDs with radius uncertainties > 20 per cent. The substellar evolutionary models are the ATMO 2020 models showing 0.1 Gyr (solid black), 0.3 Gyr (solid orange), 0.5 Gyr (dash-dotted black), 1.0 Gyr (dash-dotted orange), 5.0 Gyr (dotted black), and 10.0 Gyr (dotted orange). The COND03 models shown are 0.1 Gyr (solid light blue), 0.5 Gyr (dash-dotted light blue), and 10.0 Gyr (dotted light blue).

of those parameters. Following this change in stellar radius measurement, I find that the transiting BD in this system increases from $R_b = 0.76\,R_J$ to $R_b = 0.83\,R_J$. This change in radius ultimately does not affect the interpretation offered by Bayliss et al. (2017) that this system is old at $8.8 \pm 4.1$ Gyr, but it does clarify that it is more likely suited as a test of 4–5 Gyr substellar models rather than models examining BDs as old as 8 Gyr. My own age estimate for EPIC

I find. This smaller radius is also consistent with the a non- or less-inflated BD at a relatively long 21-day orbital period receiving little stellar flux compared to its shorter-period, equal-mass counterparts in the mass–radius diagram. For example, this is in contrast to KELT-1b, which orbits a similar star as Kepler-39b, but at a much closer 1.2-day period.

### 4.1.7 KOI-189

Aside from the publishing error in the RV data, Díaz et al. (2014) present a mass–radius determination of KOI-189b consistent with my own here. Díaz et al. (2014) emphasize that KOI-189b straddles the traditional line between BDs and low-mass stars and I support that conclusion here where I show KOI-189b to be at $M_b = 80.4 \pm 2.5\,M_J$ and a radius $R_b = 0.99 \pm 0.02\,R_J$.

### 4.1.8 KOI-205

In Díaz et al. (2013), they find a stellar radius of $R_\star = 0.84 \pm 0.02\,R_\odot$ which is 7 per cent smaller than the radius I find, $R_\star = 0.90 \pm 0.03\,R_\odot$. Given that the distance Díaz et al. (2013) use, $d = 585 \pm 16$ pc, is consistent with the distance derived from Gaia DR3, $d = 597 \pm 6$ pc, the difference in stellar radius arises not from discrepant parallax measurement, but likely from the different stellar evolutionary models used in Díaz et al. (2013) (the BT-Settl models by Allard, Homeier & Freytag 2012). Both the MIST and BT-Settl frameworks cover a stellar mass range that includes KOI-205 at $M_\star = 0.88\,M_\odot$, though the BT-Settl models reach masses well into the LTY BD regime while the MIST models are lower bound at $M_\star = 0.1 M_\odot$. Using the MIST models yields a larger estimate for the stellar radius, which increases the radius estimate for the BD from $R_b = 0.81 \pm 0.02\,R_J$ to $R_b = 0.87 \pm 0.02\,R_J$. Though a difference of $0.06\,R_J$ may seem relatively insignificant, such a change for a BD this small can noticeably impact the interpretation of the best-fitting substellar age–radius models from ATMO 2020 or COND03. At a given mass, 5–7 per cent changes in the radius at ages older than 1 Gyr can lead to different interpretations of the age by 2–5 Gyr (see the ATMO 2020 models in Fig. 4).

### 4.1.9 KOI-415

This transiting BD has the longest orbital period known to date at 166 days. The original BD radius value of $R_b = 0.79 \pm 0.12\,R_J$ made by Moutou et al. (2013) is inconsistent with my radius determination of $R_b = 0.86 \pm 0.03\,R_J$. My findings show a larger host star ($R_\star = 1.36 \pm 0.04\,R_\odot$ compared to $R_\star = 1.25 \pm 0.15\,R_\odot$) at a greater distance $d = 950 \pm 12$ pc than what Moutou et al. (2013) find, resulting in a larger transiting BD by several per cents. Moutou et al. (2013) use the Yonsei-Yale stellar isochrones from 2004 (Demarque et al. 2004) in their work, which may give rise to the radius discrepancies when compared to the MIST isochrones I make use of here.

### 4.1.10 WASP-30

The follow-up work by Triaud et al. (2013) to the original discovery work by Anderson et al. (2011) report a BD radius of $R_b = 0.95 \pm 0.03\,R_J$, which is consistent with my own findings of a radius $R_b = 0.96 \pm 0.03\,R_J$. Both previous studies cite evidence of the WASP-30 system being as young as 500 Myr based on Li 6708Å absorption seen in the stellar spectrum. Though this age estimate may be supported by the age–radius relationships from the substellar ATMO 2020 models, stellar ages up to 2 Gyr cannot be ruled out in these previous studies or this one here.

### 4.1.11 WASP-128

The BD radius determination from Hodžić et al. (2018) is consistent with my own at $R_b = 0.96 \pm 0.02\,R_J$, although I find the BD mass to be slightly higher at $M_b = 39.3 \pm 1.0\,M_J$ compared to $M_b = 37.5 \pm 0.8\,M_J$ from the original study. The original work used parallax measurements from Gaia DR2, so it was expected that the final stellar and BD parameters between that work and this one would be fairly consistent with each other.

## 4.2 Changes to the substellar mass–radius diagram

A summary of the new BD parameters in this work is shown in Table A1. One notable change to the radius distribution of transiting BDs is the increase in radii for several of the smallest known transiting BDs. These are the BDs that once occupied radii between $0.75\,R_J < R_b < 0.85\,R_J$, which is a range of radii that is predicted to comprise the oldest transiting BDs; those that are older than 5 Gyr (Baraffe et al. 2003; Phillips et al. 2020; Marley et al. 2021). Understanding these oldest and smallest BDs is as important as understanding young BDs (less than 500 Myr old) that rapidly contract because these old objects represent an extreme limit of BD evolution. Old BDs enable tests of theories for the smallest possible BDs and at which ages these smallest BD radii are expected to be reached. With this work, the subset of smallest transiting BDs that trace out the substellar age–radius models from 8–10 Gyr decreases from five objects to two. Prior to this work, KOI-205b, KOI-415b, EPIC 201702477b, TOI-148b (Grieves et al. 2021), and TOI-569b (Carmichael et al. 2020) were the transiting BDs that could comfortably be characterized as 'very old', but now only TOI-148b and TOI-569b remain in this region of age–radius space.

In each of the original studies for KOI-205b, KOI-415b, and EPIC 201702477b, and from my own stellar isochrone analysis in this work, the ages of the host stars in these systems are uncertain enough that ages as young as 5 Gyr are not ruled out at the $1\sigma$ level. This means that the stellar age (which is assumed to match the BD age) broadly makes the age–radius relationships between 5 Gyr and 10 Gyr consistent with this sample of five small transiting BDs, even when using Gaia DR3. However, the uncertainties in the ages for these systems can exceed 50 per cent, making them somewhat clumsy as tools to assess the accuracy of substellar age–radius models beyond 5 Gyr. This starkly contrasts the single-digit per cent precision of the radius measurements for these objects.

These wide age uncertainties mean that, despite very precise radius measurements, this group of BDs older than 5 Gyr cannot be used to effectively test substellar age–radius models from 5 to 10 Gyr. However, establishing precise and accurate BD radii is a key step in testing these models and until the ages of these host stars can be more precisely determined, I can only speculatively discuss the implications of this reduction in the number of objects in the small radius region ($R_b < 0.85\,R_J$) of the substellar mass–radius diagram.

These implications are: (1) that very old transiting BDs do not always reach the theoretical minimum radius predicted by these models or (2) that the minimum BD radius is not as small as previously thought and is a more complicated function of BD mass and composition. A caveat to this is that the ATMO 2020 models are not designed with the irradiated environments of transiting

BDs in mind; however, similar implications still hold true for the COND03 (Baraffe et al. 2003) and Baraffe et al. (2015) models, which do consider stellar irradiation. Additionally, this discussion omits considerations of the transiting BD metallicity, which certainly affects the radius at a given age, but to a diminished degree for BDs older than 5 Gyr (Saumon & Marley 2008; Marley et al. 2021).

Regarding the AD 3116, CoRoT-3, CoRoT-15, and Kepler-39 systems, this work sees a marked improvement in the radius precision on the BDs in these systems. AD 3116b sees a factor of 4 improvement to its radius determination, making it much more consistent with substellar age–radius predictions for its age to be 500–600 Myr, which matches the age of the star cluster, Praesepe, that the system resides in. Kepler-39b moves from being a curiously radius-inflated transiting BD to a smaller object that is more inline with substellar model predictions. However, like with CoRoT-3b and CoRoT-15b, the host star to Kepler-39b does not have a particularly well-defined age like AD 3116 does, so I am limited in the depth of conclusions that may be drawn for these three systems.

### 4.3 Summary

This work is part of a larger effort to take the transiting BD community from a place of exciting individual boutique studies to a place where we more routinely perform population statistics of various characteristics of transiting brown dwarfs. To that end, I find that the following transiting BD systems have improved accuracy and precision on their BD radius as a result of the application of data from Gaia DR3: AD 3116, CoRoT-3, CoRoT-15, EPIC 201702477, Kepler-39, KOI-205, and KOI-415. These seven systems represent a substantial fraction (20 per cent) of the known transiting BD population and their new radius measurements (all mass measurements were consistent between past works and this one) change the interpretation of the substellar mass–radius diagram as a whole. Fewer transiting BDs than previously thought occupy the radius space smaller than $R_b = 0.85\,R_J$, which is a region of the mass–radius diagram where substellar evolutionary models predict the oldest BDs to be. The remaining 4 out of 11 transiting BDs, KELT-1b, KOI-189b, WASP-30b, and WASP-128b, show consistent mass–radius determinations with their previously published works.

### DATA AVAILABILITY

The *TESS* light curve data underlying this article were accessed from the MAST at https://mast.stsci.edu/portal/Mashup/Clients/Mast/Portal.html. These data are easily accessed via a light curve management software such at `lightkurve` (Lightkurve Collaboration 2018).

The *TESS* data for AD 3116, CoRoT-3, KELT-1, KOI-189, WASP-30, and WASP-128 used for the analysis in this work will be made available in an online database accompanying this article. All other light curve and RV data are taken from their respective previous works with the exception of the RV data for the KOI-189 system, which will be made available with the new *TESS* data used. All SED, extinction, and magnitude data used in the analysis of the stellar and brown dwarf parameters are queried and properly formatted by EXOFASTv2 from their respective databases (see Section 3.1). The installation and use instructions for EXOFASTv2 can be found at https://github.com/jdeast/EXOFASTv2.

### REFERENCES

Acton J. S. et al., 2021, MNRAS, 505, 2741
Allard F., Homeier D., Freytag B., 2012, Phil. Trans. R. Soc. A, 370, 2765
Anderson D. R. et al., 2011, ApJ, 726, L19
Artigau É. et al., 2021, AJ, 162, 144
Baglin A. et al., 2006, in 36th COSPAR Scientific Assembly. COSPAR Scientific Assembly, Beijing, China, p. 3749
Baraffe I., Chabrier G., Barman T. S., Allard F., Hauschildt P. H., 2003, A&A, 402, 701
Baraffe I., Homeier D., Allard F., Chabrier G., 2015, A&A, 577, A42
Bayliss D. et al., 2017, AJ, 153, 15
Beatty T. G. et al., 2017, AJ, 154, 25
Beatty T. G., Marley M. S., Gaudi B. S., Colón K. D., Fortney J. J., Showman A. P., 2019, AJ, 158, 166
Benni P., Burdanov A., Sokov E., Barkaoui K., Team G. F., Team S., Krushinsky V., 2020, J. Am. Assoc. Var. Star Obs., 48, 104
Benz W. et al., 2021, Exp. Astron., 51, 109
Bonomo A. S. et al., 2015, A&A, 575, A85
Borsato L. et al., 2021, MNRAS, 506, 3810
Borucki W. J. et al., 2010, Science, 327, 977
Bouchy F. et al., 2011a, A&A, 525, A68
Bouchy F. et al., 2011b, A&A, 533, A83
Burrows A. et al., 2001, Rev. Mod. Phys., 73, 719
Cañas C. I. et al., 2022, AJ, 163, 89
Carmichael T. W., Latham D. W., Vanderburg A. M., 2019, AJ, 158, 38
Carmichael T. W. et al., 2020, AJ, 160, 53
Carmichael T. W. et al., 2021, AJ, 161, 97
Carmichael T. W. et al., 2022, MNRAS, 514, 4944
Choi J. et al., 2016, ApJ, 823, 102
Csizmadia S. et al., 2015, A&A, 584, A13
David T. J. et al., 2019, ApJ, 872, 161
Deleuil M. et al., 2008, A&A, 491, 889
Demarque P. et al., 2004, ApJS, 155, 667
Díaz R. F. et al., 2013, A&A, 551, L9
Díaz R. F. et al., 2014, A&A, 572, A109
Dotter A., 2016, ApJS, 222, 8
Eastman J. D. et al., 2019, preprint (arXiv:1907.09480)
Gaia Collaboration, 2022, preprint (arXiv:2208.00211)
Gillen E. et al., 2017, ApJ, 849, 11
Gossage S. et al., 2018, ApJ, 863, 67
Grieves N. et al., 2021, A&A, 652, A127
Hatzes A. P., Rauer H., 2015, ApJ, 810, L25
Hodžić V. et al., 2018, MNRAS, 481, 5091
Howell S. B. et al., 2014, PASP, 126, 398
Irwin J. et al., 2010, ApJ, 718, 1353
Irwin J. M. et al., 2018, AJ, 156, 140
Jackman J. A. G. et al., 2019, MNRAS, 489, 5146
Jenkins J. M. et al., 2016, in Chiozzi G., Guzman J. C., eds, Proc. SPIE Conf. Ser. Vol. 9913, Software and Cyberinfrastructure for Astronomy IV. SPIE, Bellingham, p. 99133E
Johnson J. A. et al., 2011, ApJ, 730, 79
Lightkurve Collaboration, 2018, Astrophysics Source Code Library, record ascl: 1812.013

Lindegren L. et al., 2021, A&A, 649, A4
Mann A. W. et al., 2019, ApJ, 871, 63
Marley M. S. et al., 2021, ApJ, 920, 85
Moutou C. et al., 2013, A&A, 558, L6
Nowak G. et al., 2017, AJ, 153, 131
Palle E. et al., 2021, A&A, 650, A55
Parviainen H. et al., 2022, A&A, 668, A93
Paxton B. et al., 2015, ApJS, 220, 15
Pepper J. et al., 2007, PASP, 119, 923
Persson C. M. et al., 2019, A&A, 628, A64
Phillips M. W. et al., 2020, A&A, 637, A38
Pollacco D. L. et al., 2006, PASP, 118, 1407
Psaridi A. et al., 2022, A&A, 664, A94
Ricker G. R. et al., 2015, J. Astron. Telesc. Instrum. Syst., 1, 014003
Saumon D., Marley M. S., 2008, ApJ, 689, 1327
Schanche N. et al., 2020, MNRAS, 499, 428
Schlafly E. F., Finkbeiner D. P., 2011, ApJ, 737, 103
Sebastian D. et al., 2022, MNRAS, 516, 636
Siverd R. J. et al., 2012, ApJ, 761, 123
Skrutskie M. F. et al., 2006, AJ, 131, 1163
Smith J. C. et al., 2012, PASP, 124, 1000
Spiegel D. S., Burrows A., Milsom J. A., 2011, ApJ, 727, 57
Stassun K. G. et al., 2018, AJ, 156, 102
Stumpe M. C., Smith J. C., Catanzarite J. H., Van Cleve J. E. , Jenkins J. M., Twicken J. D., Girouard F. R., 2014, PASP, 126, 100
Subjak J. et al., 2020, AJ, 159, 151
Triaud A. H. M. J. et al., 2013, A&A, 549, A18
Wright E. L. et al., 2010, AJ, 140, 1868
Zhou G. et al., 2019, Astron. J., 157, 31

## SUPPORTING INFORMATION

Supplementary data are available at *MNRAS* online.

**supp_data**

Please note: Oxford University Press is not responsible for the content or functionality of any supporting materials supplied by the authors. Any queries (other than missing material) should be directed to the corresponding author for the article.

## APPENDIX A: SUMMARY OF TRANSITING BROWN DWARF PARAMETERS

**Table A1.** List of published transiting brown dwarfs and very low-mass stars as of August 2022. The original discovery paper or the most recent paper is shown in the right-most column. The systems analysed in this work are in boldface in this column.

| Name | $P$ (days) | $M_{BD}/M_J$ | $R_{BD}/R_J$ | e | $M_\star/M_\odot$ | $R_\star/R_\odot$ | $T_{eff}$(K) | [Fe/H] | Ref. |
|---|---|---|---|---|---|---|---|---|---|
| HATS-70b | 1.888 | $12.9 \pm 1.8$ | $1.38 \pm 0.08$ | <0.18 | $1.78 \pm 0.12$ | $1.88 \pm 0.07$ | $7930 \pm 820$ | $+0.04 \pm 0.11$ | 1 |
| TOI-1278b | 14.476 | $18.5 \pm 0.5$ | $1.09 \pm 0.24$ | $0.013 \pm 0.004$ | $0.54 \pm 0.02$ | $0.57 \pm 0.01$ | $3799 \pm 42$ | $+0.00 \pm 0.09$ | 2 |
| **Kepler-39b** | 21.087 | $19.0 \pm 1.3$ | $1.07 \pm 0.03$ | $0.066 \pm 0.036$ | $1.20 \pm 0.09$ | $1.26 \pm 0.03$ | $6290 \pm 120$ | $+0.07 \pm 0.14$ | 3, **34** |
| GPX-1b | 1.745 | $19.7 \pm 1.6$ | $1.47 \pm 0.10$ | 0 (adopted) | $1.68 \pm 0.10$ | $1.56 \pm 0.10$ | $7000 \pm 200$ | $+0.35 \pm 0.10$ | 4 |
| **CoRoT-3b** | 4.256 | $22.3 \pm 1.0$ | $1.08 \pm 0.05$ | $0.012 \pm 0.01$ | $1.44 \pm 0.09$ | $1.66 \pm 0.08$ | $6710 \pm 140$ | $-0.04 \pm 0.08$ | 5, **34** |
| **KELT-1b** | 1.217 | $27.9 \pm 1.0$ | $1.13 \pm 0.03$ | <0.0015 | $1.39 \pm 0.07$ | $1.49 \pm 0.04$ | $6520 \pm 94$ | $+0.07 \pm 0.08$ | 6, **34** |
| NLTT 41135b | 2.889 | $33.7 \pm 2.8$ | $1.13 \pm 0.27$ | <0.02 | $0.19 \pm 0.03$ | $0.21 \pm 0.02$ | $3230 \pm 130$ | $-0.25 \pm 0.25$ | 7 |
| **WASP-128b** | 2.209 | $39.3 \pm 1.0$ | $0.96 \pm 0.02$ | <0.007 | $1.21 \pm 0.05$ | $1.18 \pm 0.02$ | $6081 \pm 78$ | $+0.12 \pm 0.09$ | 8, **34** |
| CWW 89Ab | 5.293 | $39.2 \pm 1.1$ | $0.94 \pm 0.02$ | $0.189 \pm 0.002$ | $1.10 \pm 0.05$ | $1.03 \pm 0.02$ | $5755 \pm 49$ | $+0.20 \pm 0.09$ | 9, 10 |
| **KOI-205b** | 11.720 | $39.7 \pm 2.1$ | $0.87 \pm 0.02$ | $0.026 \pm 0.018$ | $0.88 \pm 0.05$ | $0.90 \pm 0.03$ | $5238 \pm 87$ | $+0.15 \pm 0.14$ | 11, **34** |
| TOI-1406b | 10.574 | $46.0 \pm 2.7$ | $0.86 \pm 0.03$ | 0 (adopted) | $1.18 \pm 0.09$ | $1.35 \pm 0.03$ | $6290 \pm 100$ | $-0.08 \pm 0.09$ | 12 |
| EPIC 212036875b | 5.170 | $52.3 \pm 1.9$ | $0.87 \pm 0.02$ | $0.132 \pm 0.004$ | $1.29 \pm 0.07$ | $1.50 \pm 0.03$ | $6238 \pm 60$ | $+0.01 \pm 0.10$ | 10, 13 |
| TOI-503b | 3.677 | $53.7 \pm 1.2$ | $1.34 \pm 0.26$ | 0 (adopted) | $1.80 \pm 0.06$ | $1.70 \pm 0.05$ | $7650 \pm 160$ | $+0.61 \pm 0.07$ | 14 |
| TOI-852b | 4.946 | $53.7 \pm 1.4$ | $0.83 \pm 0.04$ | 0 (adopted) | $1.29 \pm 0.03$ | $1.72 \pm 0.04$ | $5750 \pm 76$ | $+0.34 \pm 0.08$ | 15 |
| **AD 3116b** | 1.983 | $54.6 \pm 6.8$ | $0.95 \pm 0.07$ | $0.144 \pm 0.045$ | $0.28 \pm 0.03$ | $0.29 \pm 0.02$ | $3165 \pm 106$ | $+0.17 \pm 0.09$ | 16, **34** |
| CoRoT-33b | 5.819 | $59.0 \pm 1.8$ | $1.10 \pm 0.53$ | $0.070 \pm 0.002$ | $0.86 \pm 0.04$ | $0.94 \pm 0.14$ | $5225 \pm 80$ | $+0.44 \pm 0.10$ | 17 |
| RIK 72b | 97.760 | $59.2 \pm 6.8$ | $3.10 \pm 0.31$ | $0.146 \pm 0.012$ | $0.44 \pm 0.04$ | $0.96 \pm 0.10$ | $3349 \pm 142$ | – | 18 |
| TOI-811b | 25.166 | $59.9 \pm 13.0$ | $1.26 \pm 0.06$ | $0.407 \pm 0.046$ | $1.32 \pm 0.05$ | $1.27 \pm 0.06$ | $6107 \pm 76$ | $+0.40 \pm 0.09$ | 15 |
| **WASP-30b** | 4.157 | $61.7 \pm 1.5$ | $0.96 \pm 0.03$ | <0.004 | $1.23 \pm 0.05$ | $1.42 \pm 0.04$ | $6208 \pm 85$ | $+0.03 \pm 0.09$ | 19, **34** |
| TOI-263b | 0.557 | $61.6 \pm 4.0$ | $0.91 \pm 0.07$ | $0.017 \pm 0.003$ | $0.44 \pm 0.03$ | $0.44 \pm 0.03$ | $3471 \pm 100$ | $+0.00 \pm 0.09$ | 20 |
| LHS 6343c | 12.713 | $62.9 \pm 2.3$ | $0.83 \pm 0.02$ | $0.056 \pm 0.032$ | $0.37 \pm 0.01$ | $0.38 \pm 0.01$ | $3750 \pm 125$ | $+0.02 \pm 0.19$ | 21 |
| TOI-569b | 6.556 | $63.8 \pm 1.0$ | $0.75 \pm 0.02$ | 0 (adopted) | $1.21 \pm 0.03$ | $1.48 \pm 0.03$ | $5705 \pm 76$ | $+0.40 \pm 0.08$ | 12 |
| TOI-2119b | 7.201 | $64.4 \pm 2.3$ | $1.083 \pm 0.03$ | $0.339 \pm 0.015$ | $0.53 \pm 0.02$ | $0.50 \pm 0.01$ | $3647 \pm 96$ | $+0.08 \pm 0.08$ | 22, 33 |
| **CoRoT-15b** | 3.060 | $64.0 \pm 5.0$ | $0.94 \pm 0.12$ | $0.042 \pm 0.039$ | $1.29 \pm 0.12$ | $1.40 \pm 0.14$ | $6340 \pm 190$ | $+0.09 \pm 0.19$ | 23, **34** |
| **KOI-415b** | 166.788 | $64.8 \pm 6.8$ | $0.86 \pm 0.03$ | $0.700 \pm 0.003$ | $0.93 \pm 0.14$ | $1.36 \pm 0.04$ | $5783 \pm 84$ | $-0.24 \pm 0.10$ | 24, **34** |
| TOI-1982b | 17.172 | $65.9 \pm 2.8$ | $1.08 \pm 0.04$ | $0.272 \pm 0.014$ | $1.41 \pm 0.08$ | $1.51 \pm 0.05$ | $6325 \pm 110$ | $-0.10 \pm 0.09$ | 25 |
| TOI-629b | 8.718 | $67.0 \pm 3.0$ | $1.11 \pm 0.05$ | $0.298 \pm 0.008$ | $2.16 \pm 0.13$ | $2.37 \pm 0.11$ | $9100 \pm 200$ | $+0.10 \pm 0.15$ | 25 |
| TOI-2543b | 7.543 | $67.6 \pm 3.5$ | $0.95 \pm 0.09$ | $0.009 \pm 0.003$ | $1.29 \pm 0.08$ | $1.86 \pm 0.15$ | $6060 \pm 82$ | $-0.28 \pm 0.10$ | 25 |
| LP 261 − 75b | 1.882 | $68.1 \pm 2.1$ | $0.90 \pm 0.02$ | <0.007 | $0.30 \pm 0.02$ | $0.31 \pm 0.01$ | $3100 \pm 50$ | – | 26 |
| NGTS-19b | 17.840 | $69.5 \pm 5.7$ | $1.03 \pm 0.06$ | $0.377 \pm 0.006$ | $0.81 \pm 0.04$ | $0.90 \pm 0.04$ | $4716 \pm 39$ | – | 29 |
| **EPIC 201702477b** | 40.737 | $70.9 \pm 2.6$ | $0.83 \pm 0.04$ | $0.228 \pm 0.003$ | $0.95 \pm 0.05$ | $1.01 \pm 0.03$ | $5542 \pm 62$ | $+0.01 \pm 0.03$ | 27, **34** |
| CoRoT-34b | 2.119 | $71.4 \pm 8.9$ | $1.09 \pm 0.17$ | 0 (adopted) | $1.66 \pm 0.15$ | $1.85 \pm 0.29$ | $7820 \pm 160$ | $-0.02 \pm 0.20$ | 28 |
| NGTS-7Ab | 0.676 | $75.5 \pm 13.7$ | $1.38 \pm 0.14$ | 0 (adopted) | $0.48 \pm 0.13$ | $0.61 \pm 0.06$ | $3359 \pm 106$ | – | 30 |
| TOI-148b | 4.870 | $77.1 \pm 5.8$ | $0.81 \pm 0.06$ | <0.01 | $0.97 \pm 0.12$ | $1.20 \pm 0.07$ | $5900 \pm 140$ | $-0.24 \pm 0.25$ | 31 |
| TOI-587b | 8.042 | $79.9 \pm 5.3$ | $1.38 \pm 0.04$ | 0 (adopted) | $2.32 \pm 0.11$ | $2.10 \pm 0.06$ | $9780 \pm 200$ | $+0.00 \pm 0.10$ | 31 |
| **KOI-189b** | 30.360 | $80.4 \pm 2.3$ | $0.99 \pm 0.02$ | $0.274 \pm 0.004$ | $0.80 \pm 0.04$ | $0.77 \pm 0.01$ | $4973 \pm 84$ | $+0.04 \pm 0.14$ | 32, **34** |
| TOI-746b | 10.980 | $82.2 \pm 4.9$ | $0.95 \pm 0.09$ | $0.199 \pm 0.003$ | $0.94 \pm 0.13$ | $0.97 \pm 0.07$ | $5690 \pm 140$ | $-0.20 \pm 0.23$ | 31 |

*Note.* References: 1-Zhou et al. (2019), 2-Artigau et al. (2021), 3-Bonomo et al. (2015), 4-Benni et al. (2020), 5-Deleuil et al. (2008), 6-Siverd et al. (2012), 7-Irwin et al. (2010), 8-Hodžić et al. (2018), 9-Nowak et al. (2017), 10-Carmichael, Latham & Vanderburg (2019), 11-Díaz et al. (2013), 12-Carmichael et al. (2020), 13-Persson et al. (2019), 14-Subjak et al. (2020), 15-Carmichael et al. (2021), 16-Gillen et al. (2017), 17-Csizmadia et al. (2015), 18-David et al. (2019), 19-Triaud et al. (2013), 20-Palle et al. (2021), 21-Johnson et al. (2011), 22-Carmichael et al. (2022), 23-Bouchy et al. (2011a), 24-Moutou et al. (2013), 25-Psaridi et al. (2022), 26-Irwin et al. (2018), 27-Bayliss et al. (2017), 28-Sebastian et al. (2022), 29-Acton et al. (2021), 30-Jackman et al. (2019), 31-Grieves et al. (2021), 32-Díaz et al. (2014), 33-Cañas et al. (2022), **34-this work**
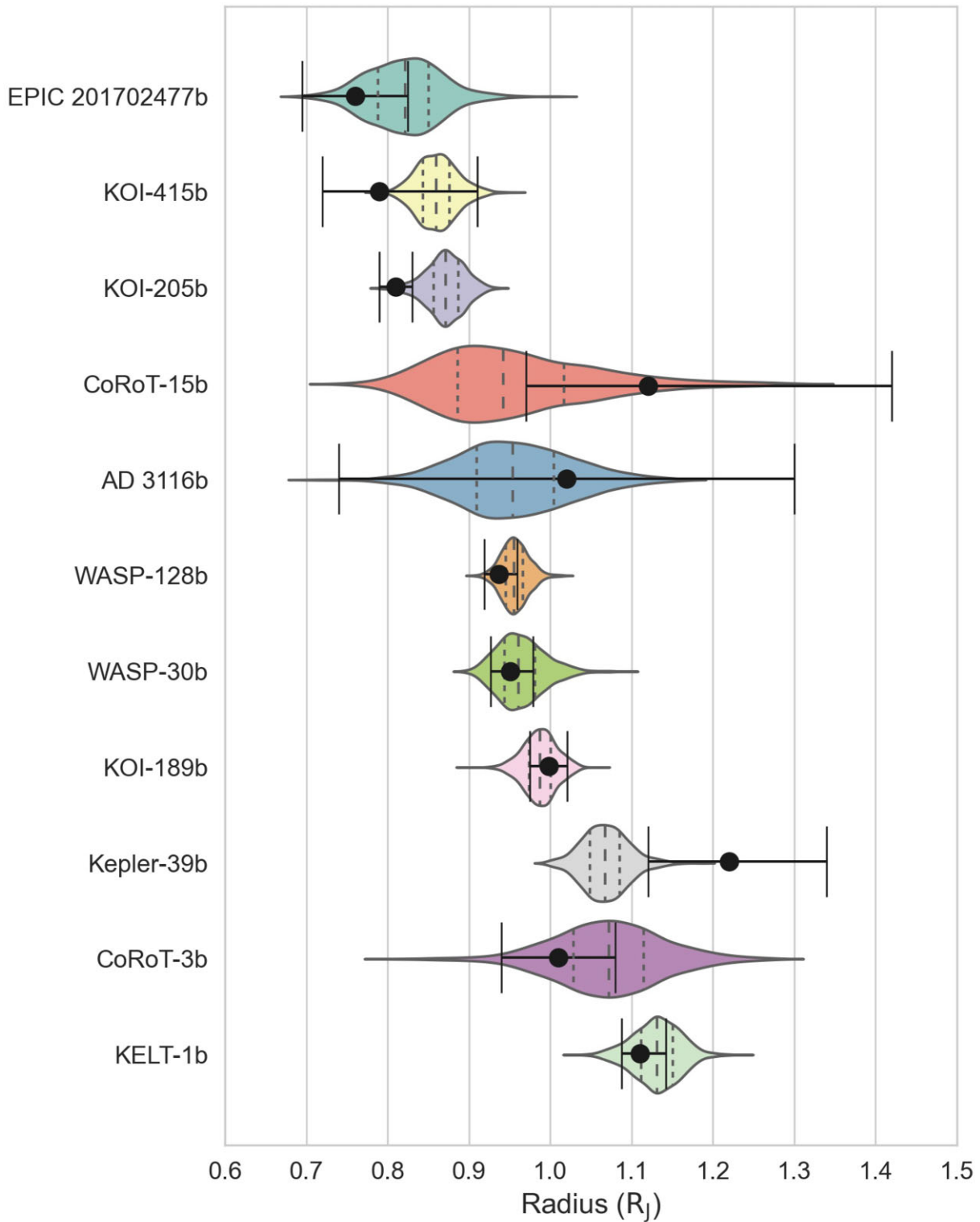
**Figure A1.** Brown dwarf radius posterior distribution functions from EXOFASTv2. Dashed lines show the median values from this work and dotted lines show the 1σ range from this work. The black points show these same metrics but for previous works.
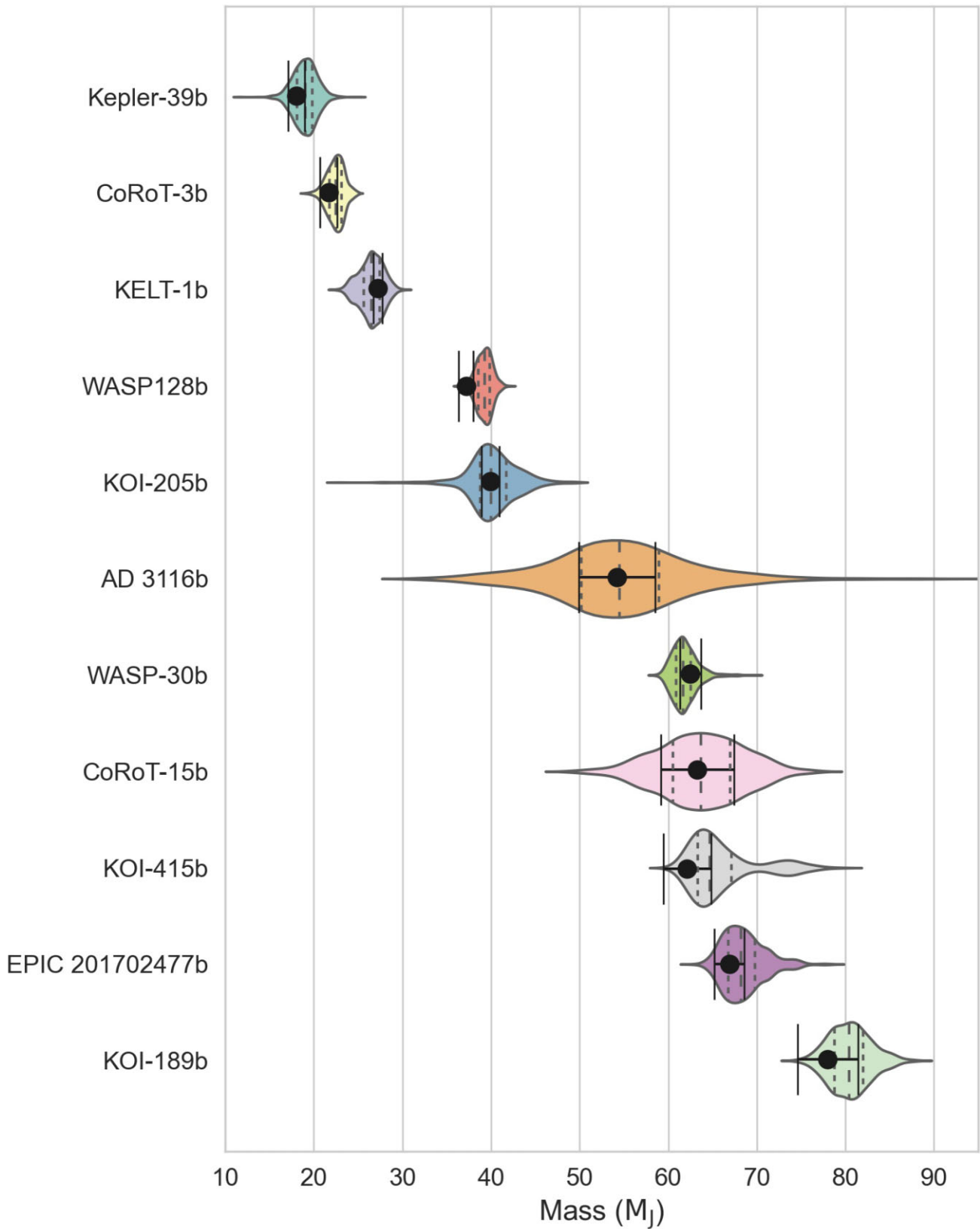
**Figure A2.** Brown dwarf mass posterior distribution functions from EXOFASTv2. Dashed lines show the median values from this work and dotted lines show the 1σ range from this work. The black points show these same metrics but for previous works.

This paper has been typeset from a TEX/LATEX file prepared by the author.